Microchimica Acta (2020) 187: 625
https://doi.org/10.1007/s00604-020-04580-5

ORIGINAL PAPER

Click chemistry reaction-triggered DNA walker amplification coupled with hyperbranched DNA nanostructure for versatile fluorescence detection and drug delivery to cancer cells

Chunli Li[1] · Hongkun Li[1] · Guifen Jie[1]

Received: 4 June 2020 / Accepted: 29 September 2020 / Published online: 23 October 2020

Abstract

A new DNA hyperbranched hybridization chain reaction (HB-HCR)-amplified fluorescence platform combined with DNA walker was developed for versatile detection of Cu^{2+}, adenosine triphosphate (ATP), and drug delivery to cancer cells. A novel click chemistry reaction-triggered DNA walking machine on magnetic beads (MBs) is introduced for the first time to convert target Cu^{2+} to lots of DNA S3 products. With the help of DNA S3 and H1 on the amino functionalized SiO_2 microsphere, HB-HCR between super hairpin DNA (SH DNA), H3-DNA, and LT-DNA was initiated to assemble a novel dendritic DNA structure with numerous fluorescent Cy5, achieving enormously amplified signal for ultrasensitive detection of Cu^{2+}. Furthermore, this contains large amounts of double-stranded DNA with plentiful GC bases, which can provide many loading sites for chemotherapeutic drug doxorubicin (Dox). The specific binding of ATP to aptamer in the dendritic DNA structure allows for release of Dox, leading to activation of Dox fluorescence for ATP assay. More importantly, this dendritic DNA nanostructure-loaded Dox enters into tumor cells by endocytosis, and then interacts with endogenous ATP, releasing Dox for efficient treatment of cancer cells. Taking advantages of these multiple amplification of HB-HCR on SiO_2 microsphere, click chemistry reaction, DNA walking, and release of Dox, this method enables ultrasensitive detection of Cu^{2+} and ATP as low as 0.1 fM and 1.0 aM, respectively, which can be widely used for accurate detection of biomolecules in clinical diagnosis and biomedical applications. This dendritic DNA nanostructure provided an effective tool for designing smart nanodevices.

Keywords Hybridization chain reaction · Click chemistry reaction · DNA walker · Hyperbranched DNA nanostructure · Drug delivery

Introduction

Copper is both an essential trace element and a toxic substance to plants, animals, and humans [1, 2]. Copper toxicosis is very rare compared to its deficiency in plants [3]. This element exhibits high toxicity to microorganisms such as algae, bacteria, viruses, and aquatic animals [4]. In addition, Cu^{2+} is also a significant environmental pollutant [5]. The U.S. Environmental Protection Agency (EPA) has set the safe limit of copper in drinking water at 1.3 mg/L (ca. 20 μM) [6]. For these reasons, the development of highly selective and sensitive detection methods for Cu^{2+} ion has great significance for environment protection and human health. As the primary energy currency, ATP plays an important role in adjusting cellular metabolizability pathways [7] and various biochemical reaction processes [8, 9]. It has been used as an indicator of living organisms for cell injury and cell viability [10]. Therefore, rapid quantification of the abundant transition metal element Cu^{2+} and the universal energy currency ATP is significant in clinical diagnosis.

To date, many analytical techniques have been developed to achieve effective detection of Cu^{2+} and ATP, such as colorimetry [11, 12], electrochemistry [13, 14], and fluorescence [15, 16]. Among them, fluorescence affords many advantages for high sensitivity, low background, low cost, and wide linear ranges. Moreover, chemistry-based recognition methods, such as specific coordination reagents [17], and Cu (I)-catalyzed

✉ Guifen Jie
guifenjie@126.com

[1] Key Laboratory of Optic-electric Sensing and Analytical Chemistry for Life Science, MOE; Shandong Key Laboratory of Biochemical Analysis; Key Laboratory of Analytical Chemistry for Life Science in Universities of Shandong; College of Chemistry and Molecular Engineering, Qingdao University of Science and Technology, Qingdao 266042, People's Republic of China

click chemistry [18] has been used in Cu^{2+} assays. The click reaction displays some advantages, such as high yields, mild reaction conditions, and well-retained framework [19, 20].

In order to improve the detection sensitivity for trace level targets, a series of powerful amplification strategies such as polymerase chain reaction [21], catalyzed assembly hairpin reaction [22], hybridization chain reaction [23], and hyperbranched hybridization chain reaction (HB-HCR) has been developed for detection [24]. Among them, HB-HCR can produce multiple dendritic DNA nanostructures with much high amplification efficiency, and has provided a useful tool for amplified sensing platform in bioanalysis [25, 26]. This dendritic DNA nanostructures with good biocompatibility and stability are also good drug delivery vehicle [27, 28], and the DNA duplex GC base pairs favorably interacts with drug Dox for self-assembly and loading, which has a clear inhibition influence on a wide range of cancers [29, 30].

In this work, we reported a novel HB-HCR cascade amplification method for versatile FL detection of Cu^{2+} and ATP activity based on Cu(I)-catalyzed click chemistry reaction. In the presence of target Cu^{2+}, DNA walking amplification based on click chemistry reaction was performed to produce lots of DNA S3. S3 opens H1 on the SiO_2 microspheres, which further initiated HB-HCR to form the dendritic DNA nanostructure with abundant fluorescent signal probes for amplified detection of Cu^{2+}. Then, large amounts of Dox were loaded into the double-stranded DNA in the nanostructure, and specific binding of ATP led to release of Dox, generating significantly amplified fluorescence signal for ATP detection. Moreover, the entrance of dendritic DNA nanostructure into cancer cells can be used for both confocal imaging and controllable drug delivery of Dox due to overexpressed ATP in cancer cells. The strategy demonstrated good property with ultrahigh sensitivity for versatile assays of Cu^{2+}, ATP, and clinical treatment of cancer cells.

Experimental section

Assembly of H1 on SiO_2 microsphere

1-Ethyl-3-(3-dimethylaminopropyl)-carbodiimide hydrochloride (EDC, 12.5 μL, 100 mM) and N-hydroxysuccinimide (NHS, 12.5 μL, 25 mM) were added to 25 μL of 2.0×10^{-7} M H1 DNA to activate the carboxyl group for 1 h, then 18 μL of amino-modified SiO_2 microspheres were added and incubated for over 6 h (37 °C). To obtain the SiO_2-H1 conjugate, excess H1 was removed by centrifuging the solution.

Fabrication of the dendritic DNA nanostructure for amplified fluorescence detection of Cu^{2+}

The obtained DNA (S3) solution and SiO_2-H1 conjugate were uniformly mixed, and incubated for 1.5 h (37 °C), unbound S3 was removed by centrifuging the solution. H2 (50 μL, 0.1 μM) was added to the above SiO_2-H1-S3 mixture, and incubated for 120 min, unbound H2 was removed by centrifuging the solution. Then, 50 μL of 5.0×10^{-7} M SH was added to the above mixture and incubated for 120 min to perform the hybridization reaction. Fifty microliters of 5.0×10^{-7} M H3 (Cy5-BHQ2) was added to the above mixture and incubated for 120 min, then 50 μL of AS1 (5.0×10^{-7} M) was added to the above mixture and incubated for 120 min to perform the hybridization reaction. LT and LA are incubated for 1 h to obtain LT/LA. Fifty microliters of 5.0×10^{-7} M LT/LA was added to the above mixture and incubated for 90 min to perform the hybridization reaction. Finally, 50 μL of 5.0×10^{-7} M AS2 was added to the above mixture and incubated for 90 min to perform HB-HCR. Unbound DNA was removed by centrifuging the solution, the precipitate was redispersed in 50 μL of ultrapure water, and the resulting mixtures were immediately subjected to fluorescence measurements.

Fabrication of the dendritic DNA nanostructure with Dox for ATP detection

Ten microliters of 100 μM Dox and the SiO_2-HB-HCR solution were mixed, and incubated for 3 h (37 °C), then excess Dox were removed by centrifugation; the precipitate was redispersed in 50 μL of ultrapure water. Ten microliters of various concentration of ATP was added to the above SiO_2-HB-HCR-Dox solution and incubated at 37 °C for 2 h, then the Dox was released. Finally, the fluorescence signal of the mixture solution was measured for assay of target ATP.

Results and discussion

Principle for the HB-HCR-based fluorescence platform for versatile detection of Cu^{2+}, ATP, and drug delivery to cancer cells

The part A in Scheme 1 displays the DNA walking amplification process based on click chemistry reaction. The amino-modified DNAzyme and S1 were first linked to the carboxyl magnetic beads by peptide bond. The magnetic beads are mainly used for magnetic separation to produce a large amount of product S3. When target Cu^{2+} and AA are present, Cu^{+} was in situ generated by Cu^{2+} reduction, then click chemistry reaction drove S1 to bind with S2; the hairpin-locked DNAzyme was opened through hybridization with S1 and S2, yielding the "active" DNAzyme, which was then

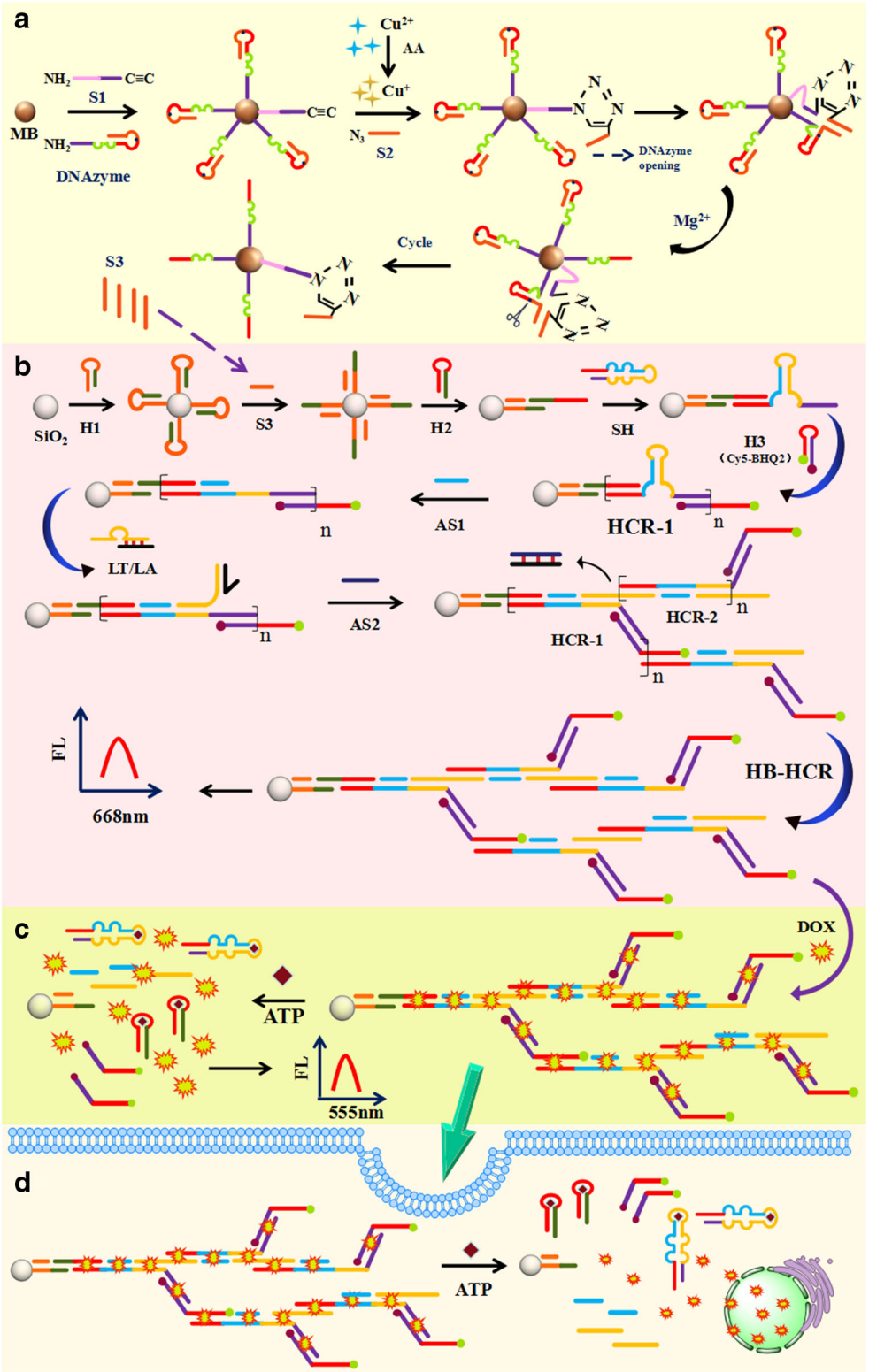

Scheme 1 Schematic illustration for (**a**) target Cu^{2+}-triggered click chemistry reaction and DNA walking amplification process on magnetic beads for generating DNA S3, (**b**) fabrication of the HB-HCR amplified fluorescence system for detecting target Cu^{2+}, (**c**) fabrication of the HB-HCR amplified fluorescence system for ATP detection, and (**d**) application of the prepared SiO_2-HB-HCR-Dox for confocal imaging and drug Dox delivery to MCF-7 cells

specifically cleaved by Mg^{2+} at the cleavage site. The released S1/S2 hybridized with another DNAzyme. Due to the DNA walking amplification on the magnetic beads, many S3 products were obtained. The part (B) shows the HB-HCR-based versatile fluorescence strategy for amplified detection of Cu^{2+}. The carboxyl-modified H1 was first linked to the amino SiO_2 microspheres by covalent bond, then S3 hybridized with H1, and opened green ssDNA of H1 further hybridized with green

segment of H2. Subsequently, the red ssDNA of H2 hybridized with red section of SH, and the opened purple ssDNA of SH hybridized with H3, so the cycling processes produced many HCR-1 for the dendritic DNA structure. When the blue ssDNA AS1 was added, the blue segment of SH was opened by hybridization. With addition of the double-stranded substrate LT/LAT, the orange segment of LT hybridized with SH DNA. Subsequently, AS2 is added to dissociate LA strand by displacement reaction, and the above cycling hybridization processes generated abundant HCR-2. Finally, the HB-HCR-based dendritic DNA structure with large amount of fluorescent signal probes (H3) was prepared for amplified detection of target Cu^{2+}. In part C, as the dendritic DNA structure contains abundant GC-rich double-stranded DNA, it is used to load a large number of Dox. The specific interaction of ATP with its aptamer destroyed the DNA structure and released Dox, leading to amplified fluorescence signal of free Dox for ATP assay. The fourth part (D) displays the application of the SiO_2-HB-HCR-Dox structure for confocal imaging and drug Dox delivery to MCF-7 cells. After incubation of SiO_2-HB-HCR-Dox with cancer cells, it can enter into the cancer cells by endocytosis. The specific binding of ATP to aptamer resulted in dissociation of dsDNA in the DNA structure, so the released Dox enters the nucleus for cell imaging and treatment of cancer cells. Thus, the novel HB-HCR-amplified fluorescence platform coupled with walking amplification was developed for versatile assays of target Cu^{2+}, ATP, and drug therapy of cancer cells.

Gel electrophoresis analysis of the DNA walking amplification process and DNA HB-HCR system

The target Cu^{2+}-triggered DNA walking amplification process was characterized by polyacrylamide gel electrophoresis (PAGE). In Fig. 1, lane M is a mark, and lanes 1 to 3 showed S1, S2, and DNAzyme. When S1 was mixed with S2, no new band appeared (lane 4), while the mixture of Cu^{2+}, AA, S1, and S2 showed a bright new band in lane 5, indicating the connection of S2 and S1 based on click chemistry reaction. When Cu^{2+}, AA, S1, S2, and DNAzyme were all mixed, both S1 and S2 hybridize with DNAzyme, generating a clear band (lane 6). By comparison, when Mg^{2+} was added into the mixture of Cu^{2+}, AA, S1, S2, and DNAzyme, a new bright band appeared at the bottom of lane 7, corresponding to the single-stranded DNA (S3) produced by DNAzyme-based shearing. The above results demonstrated the successful formation of the product S3.

The designed HB-HCR system were verified by PAGE. In Fig. 2, lanes 1 to 7 showed H1, H2, SH, H3, AS1, LT, and LA, respectively, when LT was mixed with LA, producing a distinct bright band (lane 8). Lane 9 was AS2, and when AS2 was mixed with LA, an obvious band was obtained (lane 10). In the presence of S3, H1 was opened by hybridization, and a new band with higher molecular weight (S3/H1) was obtained in line 11. When H1, S3, and H2 were all present, an obvious higher band (lane 12) was obtained due to further hybridization of S3/H1 with H2. The mixture of H1, S3, H2, and SH showed another new higher band in lane 13 for hybridization of H2 with SH. When H3 was introduced to the mixture of H1, S3, H2, and SH, the purple part of SH DNA further hybridized with H3, and a new distinct band can be observed at higher position in lane 14. By introducing AS1 to the mixture of S3, H1, H2, SH, and H3, SH is further opened by hybridization in the blue section, and a clear new band (HCR-1 DNA branch, lane 15) was obtained. When H1, S3, H2, SH, H3, AS1, and LT/LA were all mixed, the LT in the double-stranded substrate LT/LA is further hybridized with the yellow segment of SH, and a new band with a highest molecular weight was obtained (lane 16). When H1, S3, H2, SH, H3, AS1, LT/LA, and AS2 were all mixed, AS2 hybridized with LA to dissociate it from LT, generating another new band at lower position and DNA branch HCR-2 (lane 17). The above results suggest that the HB-HCR can be performed to fabricate the DNA dendritic structure for assay of S3 (Target Cu^{2+}-amplification product). Furthermore, when target ATP and the hyperbranched dendritic DNA solution were all mixed, the double-stranded DNA was dissociated, so several DNA bands with different molecular weight appeared on the lane 18.

The results of Figs. 1 and 2 proved that the designed HB-HCR-based DNA dendritic system can be technically fabricated for amplified assay of target Cu^{2+} and ATP, which can be also used for fluorescence imaging and drug application in cancer cells by releasing Dox from double-stranded DNA.

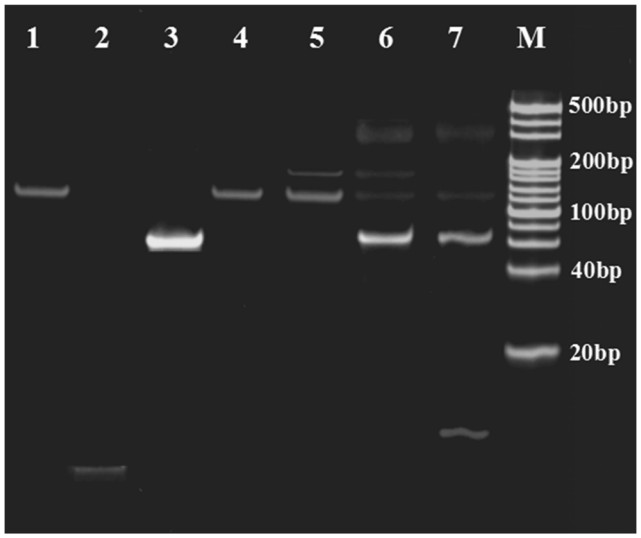

Fig. 1 Gel electrophoresis analysis of the DNA walking amplification process. Lane 1, 4 μM S1; lane 2, 100 μM S2; lane 3, 4 μM DNAzyme; lane 4, 4 μM S1 + 100 μM S2; lane 5, 4 μM S1 + 100 μM S2 + 10 μM Cu^{2+} + 20 μM AA; lane 6, 4 μM S1 + 100 μM S2 + 4 μM DNAzyme + 10 μM Cu^{2+} + 20 μM AA; lane 7, 4 μM S1 + 100 μM S2 + 4 μM DNAzyme + 1 μM Cu^{2+} + 2 μM AA + 1 μM Mg^{2+}

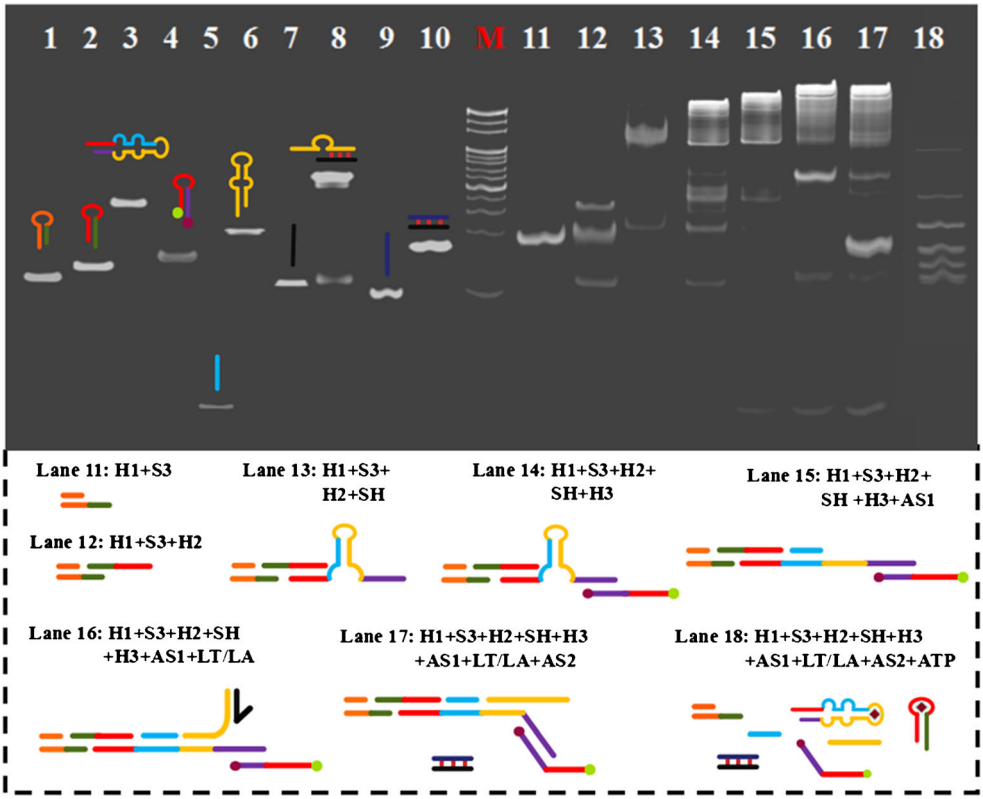

Fig. 2 Gel electrophoresis analysis of the DNA HB-HCR system. Lane 1, 2 μM H1; lane 2, 2 μM H2; lane 3, 4 μM SH; lane 4, 4 μM H3; lane 5, 100 μM AS1; lane 6, 4 μM LT; lane7, 4 μM LA; lane 8, 4 μM LT + 4 μM LA; lane 9, 4 μM AS2; lane 10, 4 μM AS2 + 4 μM LA; lane 11, 2 μM H1 + S3; lane 12, 2 μM H1 + S3 + 2 μM H2; lane 13, 2 μM H1 + S3 + 2 μM H2 + 4 μM SH; lane 14, 2 μM H1 + S3 + 2 μM H2 + 4 μM SH + 4 μM H3; lane 15, 2 μM H1 + S3 + 2 μM H2 + 4 μM SH + 4 μM H3 + 4 μM AS1; lane 16, 2 μM H1 + S3 + 2 μM H2 + 4 μM SH + 4 μM H3 + 4 μM AS1 + 4 μM LT/LA; lane 17, 2 μM H1 + S3 + 2 μM H2 + 4 μM SH + 4 μM H3 + 4 μM AS1 + 4 μM LT/LA + 4 μM AS2; lane 18, 2 μM H1 + S3 + 2 μM H2 + 4 μM SH + 4 μM H3 + 4 μM AS1 + 4 μM LT/LA + 4 μM AS2 + 1 μM ATP

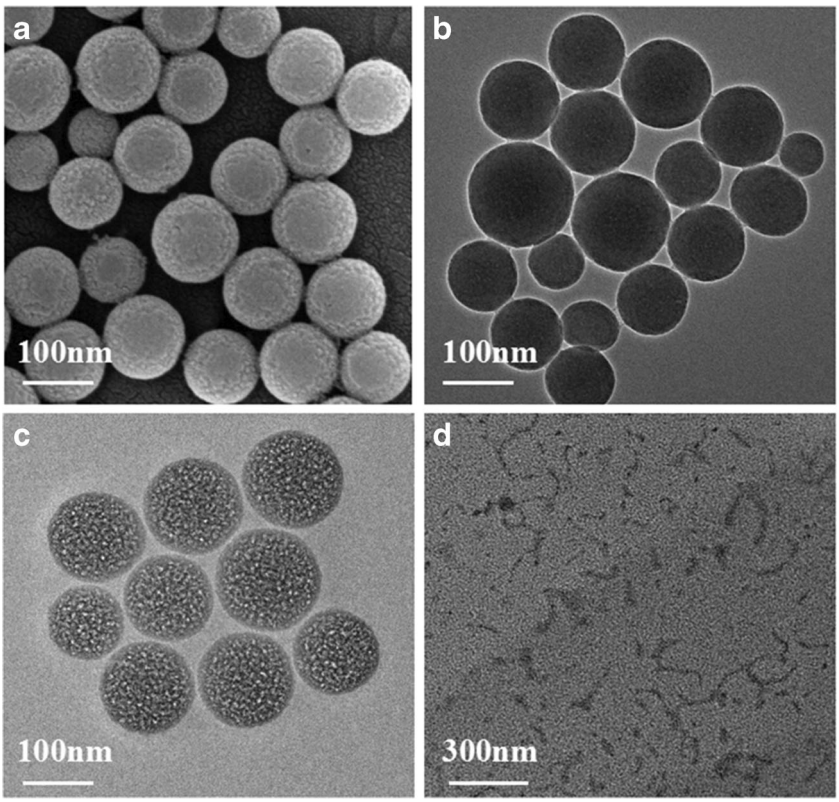

Fig. 3 **a** SEM image of SiO_2 microspheres. **b** TEM image of SiO_2 microspheres. **c** TEM image of the dendritic DNA structure on SiO_2 microspheres. **d** TEM image of the dendritic DNA structure by HB-HCR

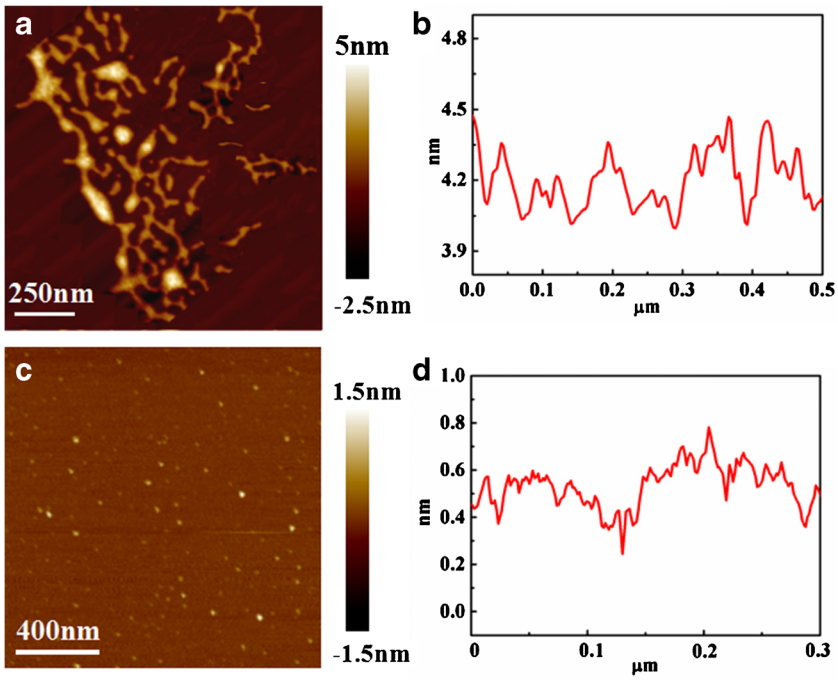

Fig. 4 **a** AFM image of HB-HCR products. **b** Height profile of HB-HCR products. **c** AFM image of ATP-HB-HCR products. **d** Height profile of ATP-HB-HCR products

Characterization of SiO_2 microspheres and HB-HCR process

The functionalized SiO_2 microspheres are used to load a large number of dendritic DNA nanostructure with many signal probes for direct fluorescence detection, and can also be centrifugated to generate precipitates, removing unbound DNA, and isolating Dox that is not embedded in double-stranded DNA. Figure 3a and b shows the SEM and TEM images of SiO_2 microspheres, respectively. The SiO_2 microspheres displayed uniform particle size with an average diameter of about 110 nm, and the surface of SiO_2 microspheres is very smooth. By comparison, when the dendritic DNA structure is formed on the SiO_2 microspheres by HB-HCR (Fig. 3c), the surface of the SiO_2 sphere became rougher. Furthermore, Fig. 3d shows the assembled DNA products by HB-HCR, and the dendritic DNA structure with an average length of 200 ± 40 nm was obviously observed, indicating that the branched DNA structure was successfully prepared by HB-HCR process.

Atomic force microscopy characterization of the HB-HCR products

To further confirm the assembled DNA products by HB-HCR, we directly visualized the morphology of the dendritic DNA structure with atomic force microscopy (AFM) imaging.

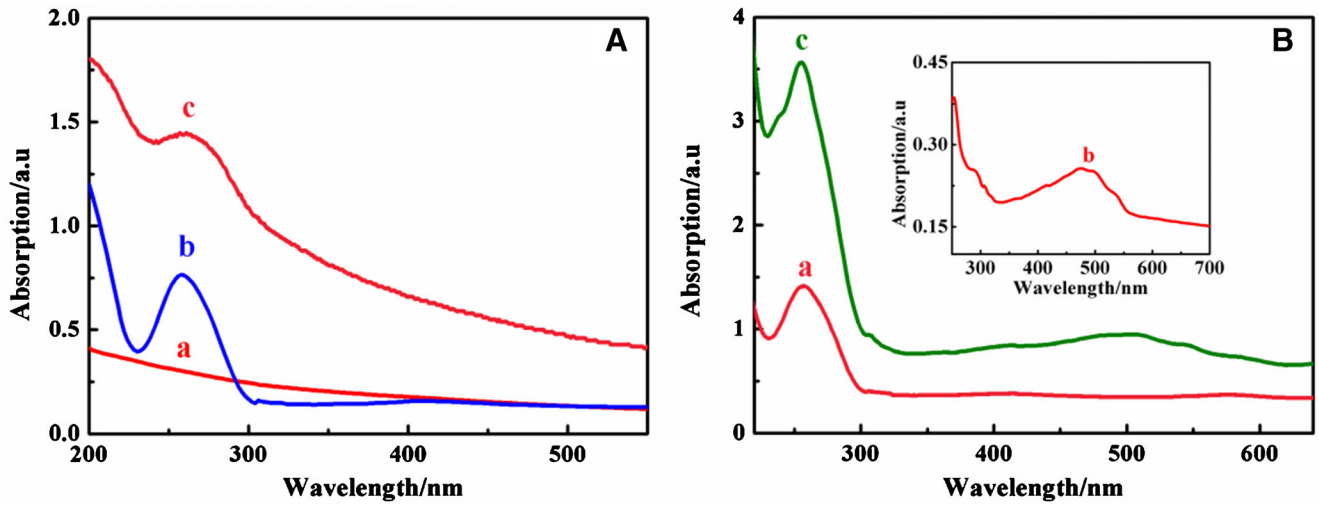

Fig. 5 UV-vis absorption spectra of (A) (a) SiO_2 microspheres, (b) H1, (c) SiO_2-H1. (B) (a) H1-S3-H2-SH-H3, (b) Dox, (c) H1-S3-H2-SH-H3-Dox

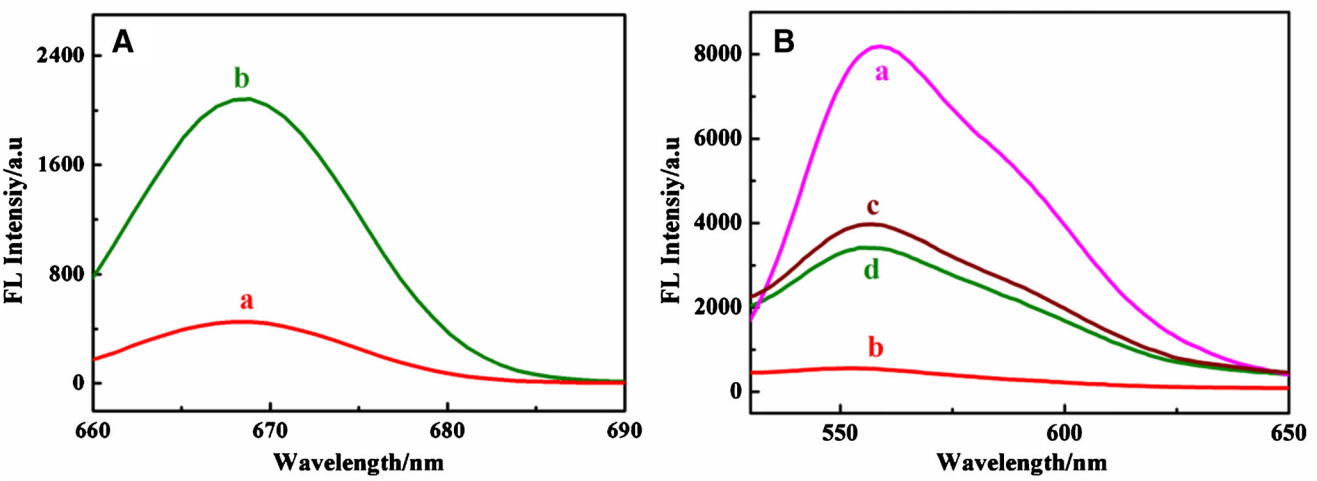

Fig. 6 (A) Feasibility of the HB-HCR-Cy5-BHQ2 fluorescence sensing system. (a) blank, (b) with 10 fM Cu^{2+}. (B) Feasibility of the HB-HCR-Dox fluorescence sensing system. (a) 10 μM free Dox, (b) blank, (c) 10 fM ATP (before centrifuge), and (d) 10 fM ATP (after centrifuge)

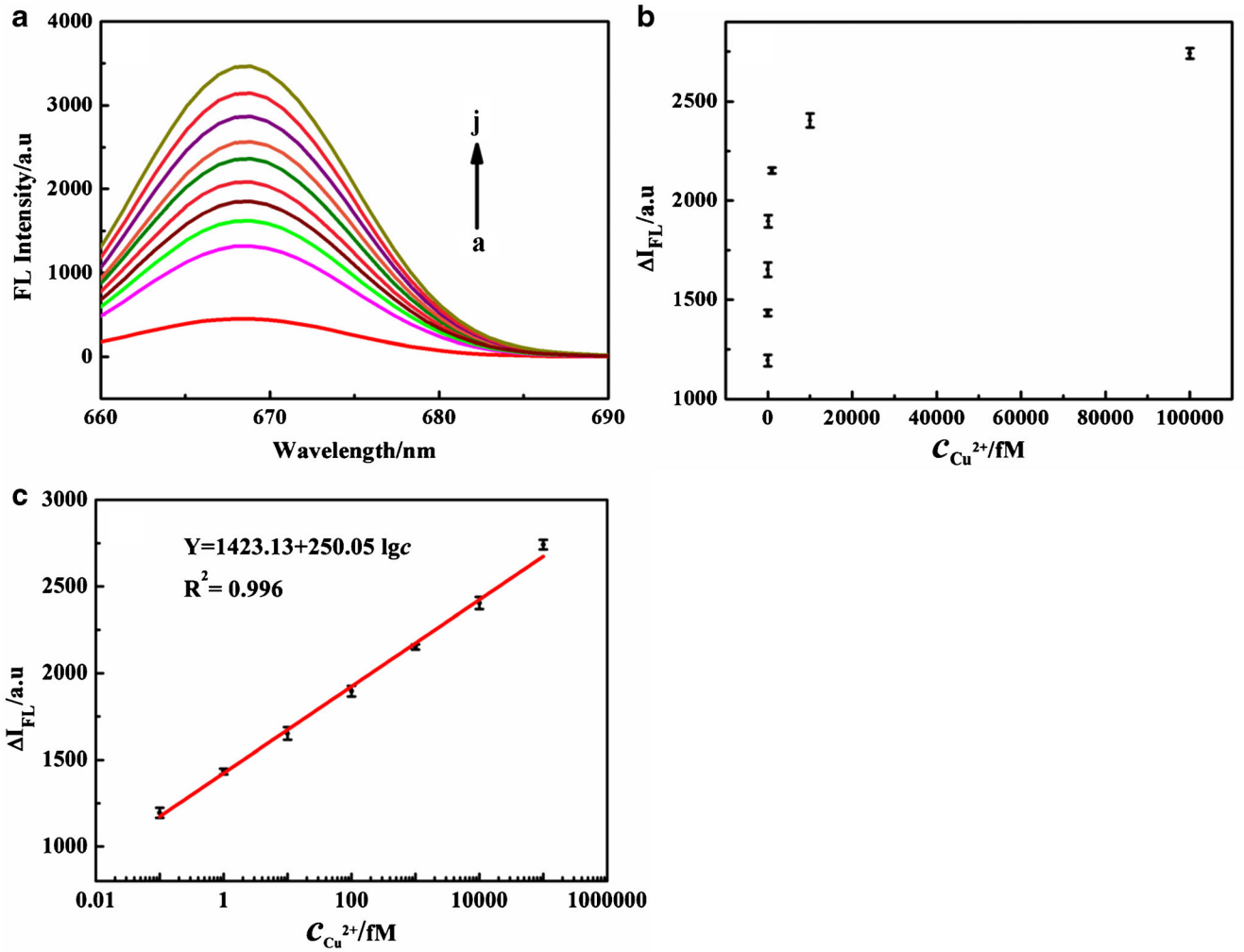

Fig. 7 **a** FL responses of the proposed strategy corresponding to different concentrations of Cu^{2+} (a to j corresponding to 0, from 10 aM to 1 nM). **b** The relationship between fluorescence signal and Cu^{2+} concentration. Inset: The linear relationship between FL intensity and logarithmic value of Cu^{2+}

Table 1 Comparison of the application performances for Cu^{2+} in our proposed FL assay with that in some previous references

Methods	Linear range, nM	Detection limit, nM	Refs
FL	10^{-7}~0.01	10^{-7}	This work
FL	30~600	0.15	[31]
FL	0.01~200	10^{-3}	[32]
ECL	0.005~900	10^{-3}	[33]
Colorimetric	3~430	1.3	[34]
SERS	0.5~1000	0.18	[35]

Table 2 Comparison of different methods for assay of ATP

Methods	Linear range, nM	Detection limit, nM	Refs
FL	10^{-9}~0.01	10^{-9}	This work
FL	0.1~125	0.081	[36]
ECL	2×10^{-5}~0.2	6.7×10^{-6}	[37]
ECL	5×10^{-3}~5	1.5×10^{-3}	[38]
PEC	5×10^{-4}~5	1.8×10^{-4}	[39]
PEC	10^{-5}~100	3.3×10^{-6}	[40]

Figure 4a displays the dendritic DNA nanostructures of different lengths, and the height is approximately 4.35 nm (Fig. 4b). In contrast, Fig. 4c displays the dendritic DNA nanostructures in the presence of ATP, some small spots instead of assembled products were observed, and the thickness was about 0.6 nm (Fig. 4d); this indicates that the specific interaction of ATP with its aptamer result in the dissociation of the DNA dendritic nanostructure. Therefore, the assembled dendritic DNA fluorescence system by HB-HCR can be used for ATP detection.

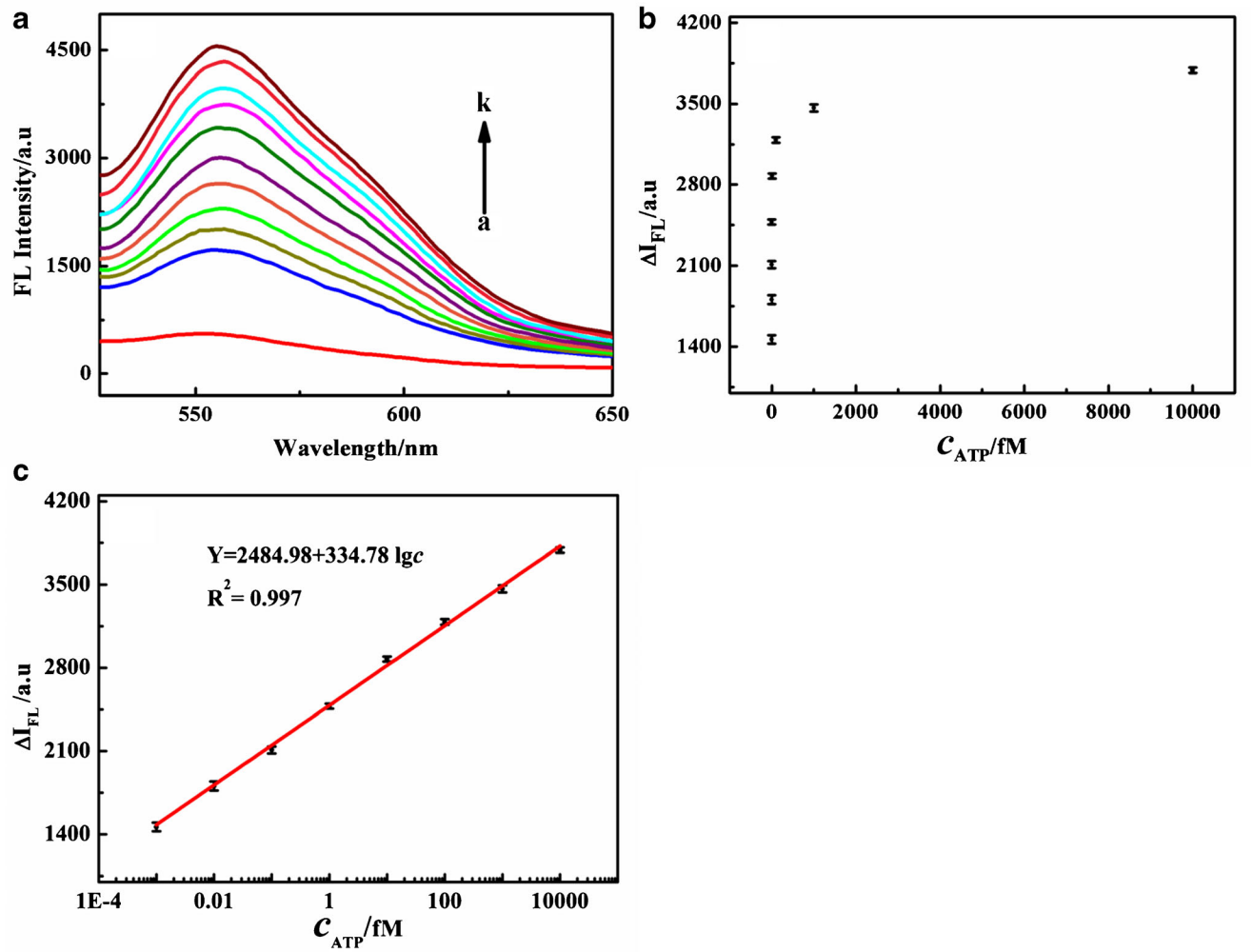

Fig. 8 **a** Fluorescence spectra of the HB-HCR-Dox system to various concentrations of ATP (a to k corresponding to 0, 0.1 aM~100 pM). **b** The relationship between the fluorescence intensity and the concentration of ATP. Inset: Linear relationship between fluorescence intensity and logarithm of ATP concentration

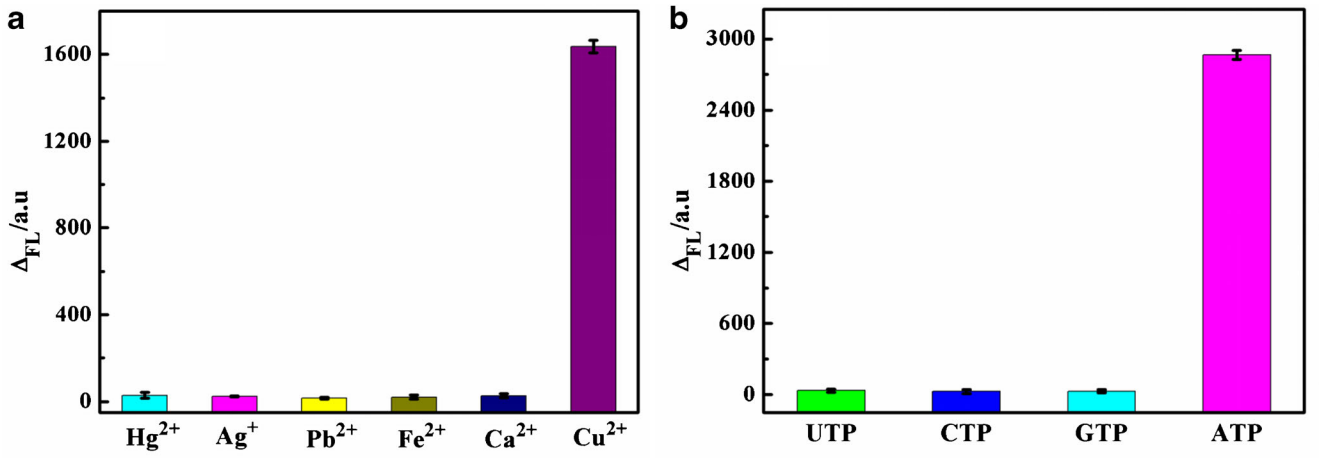

Fig. 9 **a** Selectivity of the FL strategy for detecting different metal ions (concentrations of metal ions, 10 fM). **b** Selectivity of the proposed strategy to ATP analysis (ATP concentrations, 10 fM)

Characterization of SiO_2-H1 and H1-S3-H2-SH-H3-Dox by UV-vis absorption spectra

As illustrated in Fig. 5A, curve a shows that SiO_2 microspheres have no absorbance peak, and curve b shows that H1 has an absorption peak at 260 nm. When H1 was bound to the SiO_2 microspheres, obvious absorption peak (curve c) indicated the successful conjugation of them.

In order to investigate the application of the assembled DNA nanostructure (H1-S3-H2-SH-H3) for Dox delivery to cancer cells, the assembly process of dox in H1-S3-H2-SH-H3 was characterized using absorption spectra. As illustrated in Fig. 5B, H1-S3-H2-SH-H3 showed a distinct absorption peak at 260 nm (curve a), and the anticancer drug Dox has a distinct absorption peak at 480 nm (curve b). When Dox is inserted into the dsDNA, two peaks of both DNA and Dox appeared, the peak intensity of Dox increases, and the peak position shifts red (curve c); this indicates that Dox was successfully embedded into double-stranded DNA.

Feasibility of the HB-HCR fluorescence platform for detection of target Cu^{2+}

The feasibility of the fluorescence sensing system for Cu^{2+} assay was studied. The excitation wavelength of Cy5-BHQ2 is 635 nm, and the emission peak of Cy5-BHQ2 is 668 nm. In the absence of target Cu^{2+}, the signal probes (H3) are not opened up, and there is a very low fluorescence signal (Fig. 6A, curve a, blank). When the target Cu^{2+} was present, abundant signal probes (H3) were introduced to the sensing system and opened up by HB-HCR process; therefore, obviously higher fluorescence signal was observed (curve b), indicating that the HB-HCR fluorescence sensing system can be used for target Cu^{2+} assay.

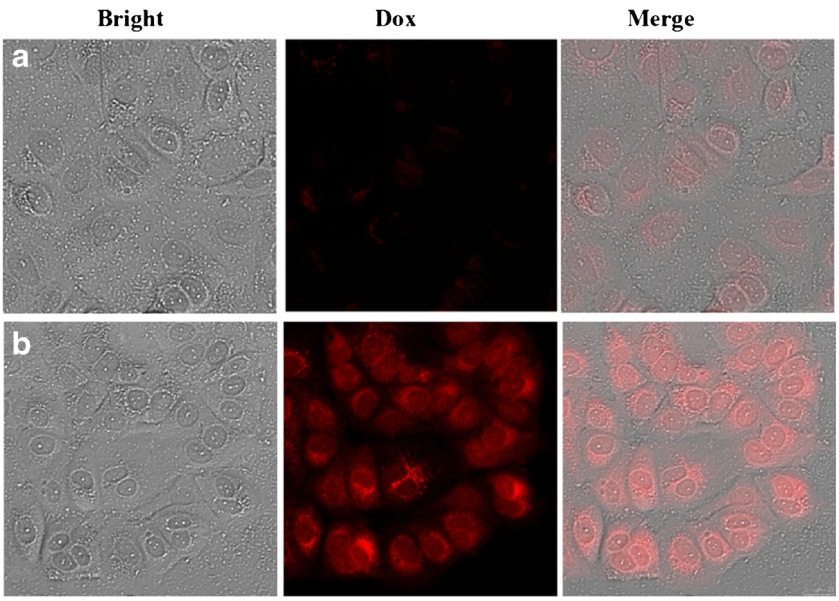

Fig. 10 Confocal microscopy images of MCF-7 cells after incubation with (**a**) 10 μM oligomycin medium and (**b**) medium, followed by incubation with SiO_2-HB-HCR-Dox

Feasibility of the HB-HCR fluorescence platform for assay of ATP

The feasibility of the fluorescence system with Dox for ATP detection was investigated. As shown in Fig. 6B, when the excitation wavelength of Dox is 480 nm, the free Dox showed very high fluorescence signal at the emission peak of 555 nm (curve a), while the HB-HCR-Dox displayed a low fluorescence signal (curve a, blank) without target ATP. The fluorescence signal of the Dox-SiO_2-HB-HCR chimera without centrifugation is shown in the curve c; therefore, obviously higher fluorescence signal was observed. When ATP was present, the interaction of ATP with its aptamer results in destruction of HB-HCR-Dox structure and release of Dox was observed that the centrifuged Dox-SiO_2-HB-HCR chimera showed obvious high fluorescence signal (curve d), indicating that the HB-HCR fluorescence sensing system can be used for ATP assay.

Analytical performance of the HB-HCR amplified fluorescence system

The performance of the proposed HB-HCR amplified fluorescence system for Cu^{2+} detection was examined. The fluorescence signal of the Cy5-based sensing system increased gradually with increasing Cu^{2+} concentration from 10 aM to 1.0 nM (Fig. 7a). Figure 7b shows that the fluorescence intensity is linearly related to the logarithmic value of Cu^{2+} concentration in the range of 0.1 fM to 100 pM, and the regression equation is $Y = 1423.13 + 250.05$ lg$c$. The calculated detection limit for Cu^{2+} is 0.1 fM (LOD = 3SB/m, where m is the slope of the corresponding calibration curve and SB is the standard deviation of the blank), indicating that the method is more sensitive than other reported strategy (Table 1). In addition, to verify the accuracy of this method, the relative standard deviation (RSD) was calculated to be 2.3% by parallel detection of 10 pM target for three times. These results indicate that the proposed strategy has well analytical performance.

Table 3 Determination of Cu^{2+} added in real water samples ($n = 3$) with the proposed strategy

Sample	Added/ fM	Obtain/ fM	Recovery/ %	RSD/ %
1	1	1.04	103.57	3.14
2	5	4.95	96.43	2.79
3	10	10.29	102.48	4.85
4	100	99.08	99.63	3.63

Table 4 Determination of ATP added in human serum samples ($n = 3$) with the proposed strategy

Sample	Added/ fM	Obtain/ fM	Recovery/ %	RSD/ %
1	1	0.94	94.72	5.11
2	5	5.04	104.45	3.25
3	10	10.08	100.07	4.03
4	100	99.04	99.31	3.48

Under the optimized conditions, the proposed strategy was used for quantitative determination of target ATP. Figure 8a shows that the FL signal of the HB-HCR-Dox increased gradually with increase of ATP concentration from 0.1 aM to 100 pM. Figure 8b shows the linear relationship between the FL signal and the logarithm of ATP concentration from 1.0 aM to 10 pM, and the linear equation is $Y = 2484.98 + 334.78$ lgc. The detection limit is 1.0 aM (LOD = 3SB/m, where m is the slope of the corresponding calibration curve and SB is the standard deviation of the blank), which is lower than that of other reported methods (Table 2). The relative standard deviation (RSD) was calculated to be 3.1% by three parallel detection of 10 pM target, demonstrating that the proposed method has good analytical performance.

Selectivity of the fluorescence strategy

The selectivity of the fluorescence strategy for Cu^{2+} was demonstrated by using Hg^{2+}, Ag^{+}, Pb^{2+}, Fe^{2+}, and Ca^{2+} as interferences. As shown in Fig. 9a, it is clear that other metal ions have no apparent fluorescence responses, while the target Cu^{2+} even at low concentration led to a significant enhanced FL signal. The results prove that the proposed strategy exhibited well selectivity.

The selectivity of the FL strategy for ATP assay was demonstrated by thymidine triphosphate analogues of GTP, UTP, and CTP. As illustrated in Fig. 9b, only ATP caused a marked fluorescence increase. It was found that no significant fluorescence signal change was obtained for CTP, GTP, and UTP in comparison with that of ATP, so the interferences were negligible for ATP analysis. The proposed strategy possesses excellent selectivity for detection of ATP.

ATP-induced drug release of the SiO_2-HB-HCR-Dox in cancer cells

We investigated ATP-triggered drug release from SiO_2-HB-HCR-Dox to MCF-7 cells. Oligomycin is a well-known inhibitor of ATP, when the cells were preincubated with oligomycin, followed by incubation with SiO_2-HB-HCR-

Dox, weak fluorescence signals were obtained (Fig. 10a). While MCF-7 cells in medium were incubated with SiO_2-HB-HCR-Dox, brighter red fluorescence signal of Dox was observed (Fig. 10b), and the Dox signal is distributed in the nucleus [41, 42], while the dispersed white small particles are SiO_2 microspheres. These results proved that the SiO_2-HB-HCR-Dox is an effective drug loading and delivery system [43, 44], and ATP can induce drug release in cancer cells. The Dox in the nucleus mainly binds with chromosomes to exert an anticancer function. These results demonstrated that the SiO_2-HB-HCR-Dox was an efficient drug Dox loading and delivery system, and the ATP in the MCF-7 cells could induce an intracellular drug release.

Application of the strategy in real samples

To further evaluate the applicability of the developed method, Cu^{2+} in water samples and ATP in human serum were detected. Cu^{2+} was not found in real water samples by our proposed method [45, 46], and 1 μL of water sample was firstly used to detect the fluorescence signal, then 1 μL of different concentrations of Cu^{2+} was added, and the fluorescence signals of the mixed solution were detected to obtain recovery rate. As can be seen from Table 3, the data from 1 to 4 showed recoveries from 96.43 to 103.57% and RSD from 2.79 to 4.85% of Cu^{2+}, confirming that the sensing platform can be used for Cu^{2+} assay in water samples.

The ATP level in human serum is about 0.94 μM [47], which is detected by our method. After the diluted human serum samples (10 μL) were spiked with different ATP samples (10 μL), the fluorescence signals of the mixture solution were measured. The data from 1 to 4 (Table 4) display the recovery of ATP in the range of 94.72–104.45% and the RSD of 3.25–5.11%, indicating that the proposed method shows good reliability and reproducibility for quantification of ATP.

Conclusions

We have developed a versatile amplified fluorescence system based on click chemistry reaction and HB-HCR for ultrasensitive detection of Cu^{2+} and ATP as well as drug delivery to cancer cells. Target Cu^{2+} firstly triggered click chemistry reaction and DNA walking amplification process to produce a lot of DNA S3. S3 then initiated HB-HCR to assemble a novel dendritic DNA nanostructure on SiO_2 microsphere, which was used to conjugate a large amount of signal probe H3 for detection of target Cu^{2+}. Furthermore, plentiful Dox is loaded into the dendritic DNA nanostructure with ATP aptamer for amplified detection of ATP and drug delivery in cancer cells. The SiO_2-HB-HCR-Dox dendritic DNA structure with abundant Dox display much high amplification efficiency, and only the released free Dox in the presence of ATP can show obvious higher fluorescence signal and effective drug effects. Based on the dual amplification strategy of the HB-HCR and DNA walker, the dendritically amplified fluorescence system enabled versatile detection of diverse targets with ultralow detection limit. Furthermore, this strategy can be used as a universal platform to detect multiple biomolecules in basic research and clinical application of drug delivery, even if a lot of DNA was used and the size of signal probe should be controlled for entering into cells.

Funding This work was supported by the National Natural Science Foundation of China (No. 21575072).

Compliance with ethical standards

Conflict of interest The authors declare that they have no competing interests.

References

1. Willis MS, Monaghan SA, Miller ML, McKenna RW, Perkins WD, Levinson BS, Bhushan V, Kroft SH (2005) Zinc induced copper deficiency: a report of three cases initially recognized on bone marrow examination. Am J Clin Pathol 123:125–131
2. Robinson NJ, Winge DR (2010) Copper metallochaperones. Annu Rev Biochem 79:537–562
3. Klevay L M (1997) Copper as a supplement to iron for hemoglobin building in the rat (Hart et al., 1928). J. Nutr
4. Lawrence C, Sanders GE, Aquatics WC (2018) Management of animal care and use programs in research, education, and testing, 2nd edn. CRC Press/Taylor &, Francis
5. Merian E (1991) Metals and their compounds in the environment. Weinheim, VCH
6. Lan G-Y, Huang C-C, Chang H-T (1257) Chem Commun 2010, 46
7. Llaudet E, Hatz S, Droniou M, Dal N, Llaudet E, Hatz S, Droniou M, Dale N (2005) Microelectrode biosensor for real-time measurement of ATP in biological tissue. Anal Chem 77:3267–3273
8. Wang J, Jiang YX, Zhou CS, Fang XH (2005) Aptamer-based ATP assay using a luminescent light switching complex. Anal Chem 77: 3542–3546
9. Deng JJ, Wang K, Wang M, Yu P, Mao LQ (2017) Mitochondria targeted nanoscale zeolitic imidazole framework-90 for ATP imaging in live cells. J Am Chem Soc 139:5877–5882
10. Eguchi Y, Shimizu S, Tsujimoto Y (1997) Intracellular ATP levels determine cell death fate by apoptosis or necrosis. Cancer Res 57: 1835–1840
11. Ge CC, Luo Q, Wang D, Zhao SM, Liang XL, Yu LX, Xing XR, Zeng LW (2014) Colorimetric detection of copper (II) ion using click chemistry and hemin/G-quadruplex horseradish peroxidase-mimicking DNAzyme. Anal Chem 86:6387–6392
12. Yin B, Ye B, Tan W, Wang H, Xie C (2009) An allosteric dual-DNAzyme unimolecular probe for colorimetric detection of copper (II). J Am Chem Soc 131:14624–14625
13. Etienne M, Bessiere J, Walcarius A (2001) Voltammetric detection of copper (II) at a carbon paste electrode containing an organically modified silica. Sensors Actuators B Chem 76:531–538
14. Yantasee W, Hongsirikarn K, Warner CL, Choi D, Addleman RS, Timchalk C (2008) Direct detection of Pb in urine and Cd, Pb, Cu, and Ag in natural waters using electrochemical sensors

immobilized with DMSA functionalized magnetic nanoparticles. Analyst. 133:348–355
15. Guo YS, Liu J, Yang GX, Sun XF, Chen HY, Xu JJ (2015) Multiple turnovers of DNAzyme for amplified detection of ATP and reduced thiol in cell homogenates. Chem Commun 51:862–865
16. He F, Wang J, Yin B, Ye B (2018) Quantification of exosome based on a copper-mediated signal amplification strategy. Anal Chem 90: 8072–8079
17. Li F, Wang J, Lai YM, Wu C, Sun SQ, He YH, Ma H (2013) Ultrasensitive and selective detection of copper (II) and mercury (II) ions by dye-coded silver nanoparticle-based SERS probes. Biosens Bioelectron 39:82–87
18. Shen QP, Li W, Tang S, Hu Y, Nie Z, Huang Y, Yao S (2013) A simple "clickable" biosensor for colorimetric detection of copper (II) ions based on unmodified gold nanoparticles. Biosens Bioelectron 41:663–668
19. Yang C, Chen K, Chen M (2019) Nanoscale metal–organic framework based two-photon sensing platform for bioimaging in live tissue. Anal Chem 91:2727–2733
20. Devadoss A, Chidsey CED (2007) Azide-modified graphitic surfaces for covalent attachment of alkyne-terminated molecules by "click" chemistry. J Am Chem Soc 129:5370–5371
21. Gao XS, Li HK, Zhao Y, Jie GF (2019) Triple-helix molecular switch-based versatile "off-on" electrochemiluminescence and fluorescence biosensing platform for ultrasensitive detection of lipopolysaccharide by multiple-amplification strategy. Biosens Bioelectron 143:111602
22. Wang H, Li C, Liu X, Zhou X, Wang F (2018) Construction of an enzyme-free concatenated DNA circuit for signal amplification and intracellular imaging. Chem Sci 9:5842–5849
23. Wu J, Li N, Yao Y (2018) DNA-stabilized silver nanoclusters for label-free fluorescence imaging of cell surface glycans and fluorescence guided photothermal therapy. Anal Chem 90:14368–14375
24. Chu Y, Deng A, Wang W (2019) Concatenated catalytic hairpin assembly/hyperbranched hybridization chain reaction based enzyme-free signal amplification for the sensitive photoelectrochemical detection of human telomerase RNA. Anal Chem 91:3619–3627
25. Bi S, Chen M, Jia X, Dong Y, Wang Z (2015) Hyperbranched hybridization chain reaction for triggered signal amplification and concatenated logic circuits. Angew Chem Int Ed 54:8144–8148
26. Xuan F, Fan TW, Hsing IM (2015) Electrochemical interrogation of kinetically-controlled dendritic DNA/PNA assembly for immobilization-free and enzyme-free nucleic acids sensing. ACS Nano 9:5027–5033
27. Schüller VJ, Heidegger S, Sandholzer N (2011) Cellular immunostimulation by CpG-sequence-coated DNA origami structures. ACS Nano 5:9696–9702
28. Hu Y, Chen Z, Zhang H, Li M, Hou Z, Luo X, Xue X (2017) Development of DNA tetrahedron-based drug delivery system. Drug Delivery 24:1295–1301
29. Zhang Y, Huang F, Ren C (2017) Targeted chemo-photodynamic combination platform based on the DOX prodrug nanoparticles for enhanced cancer therapy. ACS Appl Mater Interfaces 9:13016–13028
30. Qiu L, Chen T, Öcsoy I, Yasun E, Wu C, Zhu G, You M, Han D, Jiang J, Yu R, Tan W (2015) A cell-targeted, size-photocontrollable, nuclear-uptake nanodrug delivery system for drug-resistant cancer therapy. Nano Lett 15:457–463
31. Jin LH, Han CS (2014) Ultrasensitive and selective fluorimetric detection of copper ions using thiosulfate-involved quantum dots. Anal Chem 86:7209–7213
32. Xiong YM, Meng PJ, Li HL, Hu Y, Zhou LH, Jiang SQ, Pang YF, Li SJ, Huang PL (2018) Dual signal amplification strategy for high-sensitivity detection of copper species in bio-samples with a tunable dynamic range. Chem Commun 54:2542–2545
33. Jin JC, Wu J, Yang GP, Wu YL, Wang YY (2016) A microporous anionic metal–organic framework for a highly selective and sensitive electrochemical sensor of Cu^{2+} ions. Chem Commun 52:8475–8478
34. Cai Y, You J, You Z, Dong F, Du S, Zhang L (2018) Profuse color-evolution-based fluorescent test paper sensor for rapid and visual monitoring of endogenous Cu^{2+} in human urine. Biosens Bioelectron 99:332–337
35. Wang Y, Su Z, Wang L, Dong J, Xue J, Yu J, Wang Y, Hua X, Wang M, Zhang C (2017) SERS assay for copper (II) ions based on dual hot-spot model coupling with MarR protein: new Cu^{2+}-specific biorecognition element. Anal Chem 89:6392–6398
36. Chen JY, Ji XH, Tinnefeld P, He ZK (2016) Multifunctional dumbbell-shaped DNA-templated selective formation of fluorescent silver nanoclusters or copper nanoparticles for sensitive detection of biomolecules. ACS Appl Mater Interfaces 8:1786–1794
37. Dong YP, Zhou Y, Wang J, Zhu JJ (2016) Electrogenerated chemiluminescence resonance energy transfer between Ru $(bpy)_3^{2+}$ ECL and gold nanoparticles/graphene oxide nanocomposites with graphene oxide as coreactant and its sensing application. Anal. Chem. 88:5469–5475
38. Lu JJ, Yan M, Ge L, Ge SG, Wang SW, Yan JX, Yu JH (2013) Electrochemiluminescence of blue-luminescent graphene quantum dots and its application in ultrasensitive aptasensor for adenosine triphosphate detection. Biosens. Bioelectron. 47:271–277
39. Fan GC, Zhao M, Zhu H, Shi JJ, Zhang JR, Zhu JJ (2016) Signal-on photoelectrochemical aptasensor for adenosine triphosphate detection based on sensitization effect of CdS: Mn@Ru$(bpy)_2$ (dcbpy) nanocomposites. J Phys Chem C 120:15657–15665
40. Li MJ, Zheng YN, Liang WB (2017) Using p-type PbS quantum dots to quench photocurrent of fullerene–Au NP@ MoS_2 composite structure for ultrasensitive photoelectrochemical detection of ATP. ACS Appl Mater Interfaces 9:42111–42120
41. Zhang X, Xi Z, Gao FL (2019) Gold cube-in-cube based oxygen nanogenerator: a theranostic nanoplatform for modulating tumor microenvironment for precise chemo-phototherapy and multimodal imaging. ACS Nano 13:5306–5325
42. Zhang X, Machuki JOA, Pan WZ (2020) Carbon nitride hollow theranostic nanoregulators executing laser-activatable water splitting for enhanced ultrasound/fluorescence imaging and cooperative phototherapy. ACS Nano 14:4045–4060
43. Yao Y, Zhao D, Li N (2019) Multifunctional Fe3O4@polydopamine@DNA-fueled molecular machine for magnetically targeted intracellular Zn2+ imaging and fluorescence/MRI guided photodynamic-photothermal therapy. Anal Chem 91:7850–7857
44. Yao Y, Li N, Zhang X (2019) DNA-templated silver nanocluster/porphyrin/MnO_2 platform for label-free intracellular Zn^{2+} imaging and fluorescence−/magnetic resonance imaging-guided photodynamic therapy. Anal Chem 11:13991–14003
45. Qing M, Xie SB, Cai W (2018) Click chemistry reaction-triggered 3D DNA walking machine for sensitive electrochemical detection of copper ion click chemistry reaction-triggered 3D DNA walking machine for sensitive electrochemical detection of copper ion [J]. Anal Chem 90:11439–11445
46. Wang YL, Su ZH, Wang LM (2017) SERS assay for copper(II) ions based on dual hot-spot model coupling with MarR protein: new Cu^{2+}-specific biorecognition element [J]. Anal Chem 89: 6392–6398
47. Zhang HD, Liu YJ, Zhang K (2018) Single molecule fluorescent colocalization of split aptamers for ultrasensitive detection of biomolecules [J]. Anal Chem 2018(90):9315–9321